DOI: 10.26599/FSHW.2024.9250057

Contents lists available at SciOpen

Food Science and Human Wellness

journal homepage: https://www.sciopen.com/journal/2097-0765

Ferritin nanocage loading LYC for improving BBB transcytosis and attenuating D-gal-induced apoptosis in PC12 cells

Xiaoyu Xia [1,2,3], Han Li [1,2,3], Xianbing Xu [1,2,3], Zhenyu Wang [1,2,3], Junjie Yi [4], Guanghua Zhao [5], Ming Du [1,2,3,*]

[1] *School of Food Science and Technology, Dalian Polytechnic University, Dalian 116034, China;*

[2] *Collaborative Innovation Centre of Provincial and Ministerial Co-construction for Seafood Deep Processing, Dalian 116034, China;*

[3] *National Engineering Research Centre of Seafood, Dalian 116034, China;*

[4] *Faculty of Food Science and Engineering, Kunming University of Science and Technology, Kunming, 650500, China;*

[5] *College of Food Science and Nutritional Engineering, China Agricultural University, Beijing 100083, China.*

ABSTRACT: Aging is a physiological process that leads to degeneration and functional decline of the brain. This is accompanied by intracellular peroxidation and neuronal apoptosis. Natural antioxidants possess a remarkable effect on attenuating the oxidative stress cascade and apoptosis of neurons; however, the challenge of using natural antioxidants for neuroprotection is fabricating a delivery system to overcome the blood-brain barrier (BBB) transport. Herein, we successfully created a stable delivery platform built on rigid ferritin nanocage loading natural lycopene (LYC) molecules, crossing the BBB in quantity and being taken up in neurons. This nanoparticle worked on D-galactose-induced senescence via alleviating neuronal hyperoxidation injury and weakening neuronal apoptosis in PC12 and BV2 cells. More importantly, this natural delivery system possesses inherent biocompatibility and potential application in improving the bioavailability of bioactive edible compounds with low water solubility. This study demonstrated the effectiveness of natural antioxidant nanomedicines in maintaining the defenses of intracerebral peroxidation and improve degenerating neurons, providing the potential to combat further imbalances of neuronal microenvironment in aging neuropathy.

Keywords: ferritin; lycopene; nanocarrier; neuroprotection; aging

1. Introduction

Aging is an inevitable physiological degradation process with the passage of time, accompanying by the decline of brain function, which manifested as increased oxidative stress, loss of neurons, decreased nerve conduction, memory decline, etc [1]. As the elderly population increases, the number of patients with neurodegenerative diseases increases. Therefore, it is urgent to consider an effective neuroprotective therapy. Accumulating evidence indicates that the overproduction of reactive oxygen species (ROS) triggering intracellular peroxidation and cascade, is a major driving force of degenerative neuronal microenvironment, making ROS potential therapeutic targets. For example, artificial cascade nanozymes with superoxide dismutase (SOD) and catalase (CAT) activities can significantly reduce mitochondrial oxidative damage by

***Corresponding author**
Ming Du, Email: duming@dlpu.edu.cn

Received 4 June 2023
Received in revised from 23 July 2023
Accepted 22 August 2023

removing excessive mitochondrial superoxide [2], thereby altering microglial phenotypes and improving homeostasis in the brain [3, 4]. Considering that engineered nanocomposites suffer from pathetic biocompatibility, low brain-to-blood ratio, inadequate ROS scavenging, difficult synthesis and big size (> 10 nm) [5, 6], a fast and metabolizable synthetic strategy for the brain accumulation and effective ROS elimination is urgently needed [7].

Natural antioxidant drugs improve immunity in patients during long-term treatment of lesions with complex pathogenesis [8]. Particularly, lycopene (LYC), the most efficient carotenoid that inhibits singlet oxygen ($^1O_2$), reportedly mediates the inhibition of the oxidative stress cascade, apoptosis of neurons, neuroinflammation, and damage to mitochondria [9, 10]. What's more, it alleviates the fading cognitive of rodents under adverse physical status including aging, diabetes, and high-calorie diet [11]. However, LYC's pathetic bioavailability and poor permeability at blood-brain barrier (BBB) limit its effectiveness in neurons [12, 13], making a suitable carrier necessary to protect and enrich it to amplify its function in the brain.

Recently, nanotechnology has been extensively studied as a comprehensive treatment for complex diseases, especially degenerative neurological disease [14-16]. An ideal nano-delivery platform should possess high circulation stability in suitable size for penetration and facilitate the targeted delivery of loaded drugs to specific lesions without changing the functional properties of its cargo. Among them, protein nanocages with reversible self-assembly characteristics provide protective barriers and chemical binding sites for loaded molecules, which is a reliable way for the stable delivery of active small molecules [17]. Moreover, nanoparticles designed to regulate the neuronal microenvironment with excellent biocompatibility, such as recombinant human H-ferritin (rHuHF), will cross the BBB through its endogenous receptor-mediated endocytosis [18]. rHuHF has been successfully engineered to treat glioma and cerebral malaria [15, 19]. Taken together, a combined approach utilizing nanoparticles to promote BBB transcytosis and natural antioxidants to scavenge ROS appears to be a promising strategy for neuroprotection.

In this study, we utilized the rHuHF nanocage as the optimal carrier for constructing natural antioxidant rHuHF-LYC nanoparticle for the first time. In a typical process, the rHuHF was synthesized from the naturally encoded H-ferritin gene in humans following heterologous expression. We loaded LYC molecules into the stable cavity of rHuHF based on simulated interaction analysis and pH-responsed reversible assembly of rHuHF. The BBB transcytosis model, subcellular fluorescence localization, and antioxidant activity of rHuHF-LYC were evaluated to validate the neuro-improving efficacy of rHuHF-LYC. rHuHF-LYC provides an effective strategy for brain neuroprotection and anti-aging.

2. Materials and methods

2.1. Materials and reagents

The engineering strain BL21-pET3a-rHuHF constructed to obtain the target protein was kept at Pro. Du's laboratory in Dalian Polytechnic University (Dalian, China). The key plasmids were obtained from Sangon Biotech (Shanghai, China) and the kits utilized to construct and verify the plasmids were obtained

from Takara Co (Japan). The extraction and purification of rHuHF relied on anion exchange column and molecular sieve chromatography from GE Healthcare Bio-Sciences AB (Beijing, China). Culture products essential for cell growth were purchased from Gibco (USA). Dyes including Lyso-Tracker Red, DCFH-DA, Mito-Tracker Red CMXRos and DAPI were obtained from Beyotime (Shanghai, China). The apoptosis related antibodies were bought from Abcam (UK) and CST (UA): p-AKT (4060T), Bad (9239T), Bcl-xL (2764T), Bcl-2 (3498T), Bax (2772T), Cleaved Caspase-3 (9664T), p53 (ab33889).

2.2. The construction of rHuHF-LYC nanoparticles

rHuHF was produced by heterologous expression, during which the key parameters for the mass expression of rHuHF by engineered strains has been improved in the previous report [20]. BL21-pET3a-rHuHF strains were cultivated at 37 ℃ with ampicillin sodium (AMP) in working concentration (135 μmol/L). When the bacterial solution reached an absorbance of 0.9, rHuHF expression was induced with 500 μmol/L Isopropyl β-D-thiogalactopyranoside (IPTG) and lasted for 9 h. After screening by anion-exchange and molecular exclusion chromatography, the purified rHuHF was identified as electrophoretic pure using SDS-PAGE and Native-PAGE [21, 22].

The encapsulation of LYC benefited from the reversible self-assembly of rHuHF nanocages, adapted from our previous approach [21]. Comprised of 24 identical subunits, the globular apoferritin (12 nm) was dissociated into subunits in extreme conditions (pH ≤ 2.8 or pH ≥ 10.6) and it was reconstituted upon continuous pH adjustment to ~7.0 without denaturation. Therefore, the dissolved LYC (the particle ratio between rHuHF and LYC = 1: 100) in DMSO (1% incorporated into system) was added slowly at pH 10.6 and embedded into rHuHF nanocages after the reconstitution of rHuHF. The solution of rHuHF-LYC nanoparticles was aged away from light at 4 ℃ for 2 h. Then the resulting solution was dialyzed after centrifugation to remove insoluble LYC.

$$\text{Encapsulation efficiency} = \frac{\text{rHuHF encapsulated LYC}}{\text{total amount of LYC}} \times 100\%$$

$$\text{Loading efficiency} = \frac{\text{rHuHF encapsulated LYC}}{\text{ferritin}} \times 100\%$$

2.3. The interaction analysis between LYC and rHuHF nanocage

Discovery Studio (2017 R2) was employed to analyse the possible interaction mechanisms between LYC and rHuHF. PDB database and PyMOL 1.1 software were recruited to confirm the structure of rHuHF (PDB: 2FHA). After optimization of the structure of LYC by minimizing energy, the docking sites on the receptor (rHuHF) and the binding conformation of LYC with the highest score were calculated. Infrared spectrum and isothermal titration calorimetry (ITC) were used to verify the combination of the two molecules. The titration equilibrium was completed with the stir rate of 125 r/min at 25 ℃. The injections of LYC (60 μL, 0.2 mmol/L) were administered 30 times into the reaction pool with rHuHF (350 μL, 2 μmol/L).

2.4. Stability test of rHuHF-LYC

rHuHF-encapsulated LYC samples were incubated in a 37 ℃ water bath in dark condition. The content of LYC was measured at hourly intervals for 7 h. Free LYC was used as a control. The optimal reaction model following the first-order degradation reaction during thermal processing was shown as below [12].

$$y = a - b \times \ln(x + c)$$

where y represents the percentage of residual LYC concentration (%), x represents the treatment time of every group (h).

Formula for LYC group (R^2 = 0.9558):

$$y = 86.43537 - 4.243 \times lnx$$

Formula for rHuHF-LYC group (R^2 = 0.9945):

$$y = 90.65011 - 3.34403 \times \ln(x - 0.9281)$$

The reservation of the oxidation resistance of the encapsulated compounds was reflected though the DPPH inhibition. Every 100 μL of the DPPH dissolved in ethanol was added into 100 μL of rHuHF-LYC (2 μmol/L in 20 mmol/L Tris-HCl, pH 7.5) incubated in 96-well plates at 37 ℃. The measurement was performed at 520 nm for 1.5 h separated by every 15 min. A blank sample contained 100 μL DPPH solution in ethanol. All the samples were put under reduced light. DPPH inhibition was repeated in triplicate and the formulas below were utilized for quantitative calculation.

$$DPPH\ \ inhibition\ \ (\%) = \frac{AB - AE}{AB}\ \times\ 100$$

where, AB: OD_{520} nm of the blank group; AE: OD_{520} nm of the sample groups.

2.5. BBB transcytosis test in vitro

In vitro BBB models were built using mouse BBB endothelial cells (EC) bEnd.3 cells, human BBB EC hCMEC/D3 cells and PC12 cells (lower chamber) with reference to previous reports [16, 23]. Briefly, FITC-rHuHF-LYC/FITC-LFn (40 nmol/L) was added into BBB EC monolayer coated transwells when the transendothelial electrical resistance (TEER) reached 170 Ω·cm^2. After 2 h cultivation, the liquids in upper and lower chambers were measured respectively via the Fluorescence Spectrophotometer. The cells in upper and lower chambers were also collected and detected.

2.6. Analysis of cellular localization and uptake

The cellular localization and uptake of rHuHF-LYC were studied by the confocal laser scanning microscope (CLSM, Zeiss LSM880). BBB EC/PC12 cells were cultivated in CLSM dishes for 24 h before incubation with FITC-rHuHF-LYC/anti-human TfR1 monoclonal antibody/FITC. After 2 h, the lysotracker red probe was transferred into cells for 5 min. After washing by PBS, cells were fixed by 4% paraformaldehyde and then stained by 4′,6-diamidino-2-phenylidole (DAPI) for 5 min. The fluorescence signals were tracked with 63× oil lens. Three tests with more than 10 cells quantified per test were recorded.

2.7. Analysis of cellular peroxidation and apoptosis

The cells were cultured stably in 24-well plates for 24 h and protected by different concentrations of rHuHF-LYC. Then, D-galactose (D-gal) with suitable concentration (optimized) was utilized to stimulate

oxidative stress and damage for 4 h. ROS in PC12 and BV2 cells was reflected by DCFH-DA fluorescent probe, referring to Zhang et al [2]. The fluorescence intensity was measured at excitation wavelength of 485 nm and emission wavelength of 525 nm. Mitochondrial membrane potential and apoptosis of cells were measured according to manufacturer's protocol. To detect the superoxide dismutase (SOD) activity and neuron cholinergic activity, the cells were lysed with RIPA containing PMSF (1 mmol/L) at 4 ℃ for 30 min. Then, the cells were collected for determining SOD, Ach, and AChE activity according to the instructions of SOD kit, ACh kit, AChE kit and BCA kit.

2.8. Analysis of apoptotic signalling pathways in PC12 cells

The cell samples were ground in an ice bath and dissolved in the solution of lysis for 30 min. The collected lysates were sonicated to ensure fragmentation of the cells and then was centrifuged (12000 g, 15 min, 4 ℃). The proteins in the supernatant were denatured and levelled in concentration. SDS-polyacrylamide gel was utilized to separate various proteins, allowing the individual target protein transferring to PVDF membrane for subsequent binding with the corresponding antibodies. The membrane was incubated with primary antibodies overnight and was then bound to the secondary antibody for 2 h after a three-time wash interval. ECL staining reagent was used to visualize the bands. The gray values were quantified by Fiji and normalized by β-actin.

2.9. Statistical analysis

Data plots were generated using Origin, GraphPad Prism and Fiji softwares. Statistical significance ($P < 0.05$) was generated from more than two replicates of each data. The structure of the biopolymer (rHuHF) was characterized by PyMOL software.

3. Results and discussion

3.1. Construction and characterization of rHuHF-LYC nanoparticles

Compared to the naturally occurring heterozygous ferritin gene, the H-chain gene of homozygous ferritin was defined to be highly expressed in a cDNA library [24], based on which rHuHF nanocages were produced by the heterologous expression process. The purified rHuHF (approximately 480 kDa) was formed by only one subunit of approximately 20 kDa (Figure 1C), which was in good agreement with previous findings [20]. The stable rHuHF nanocage with its nondenaturing dissociation and reassembly properties, serves as the nanocarrier for housing and protecting encapsulated acitve molecules [25]. Furthermore, LYC was wrapped by rHuHF into its internal cavity and stably existed in its cavity because the size of LYC (33.3 Å in length and 10.9 Å in width) was far beyond the channels (3-4 Å) on the surface of rHuHF (Figure 1A). In this case, the encapsulation and loading efficiencies were 60.64% and 6.06% (Figure 1B), respectively, i.e., the particle ratio of LYC/rHuHF on average was 56:1 on average, that was much more than that of curcumin, rutin, β-carotene, and other insoluble substances [20, 22, 26]. It can be clearly observed that the aqueous solution of rHuHF is clear and transparent, and the rHuHF-LYC solution appears uniform and bright red, while the free LYC is suspended as solid particles (Figure 1B). Moreover, the nanoparticles still

possessed an all-right nanocage morphology and a uniform diameter (Figure 1D). A slight expansion of the nanocage size explained their size flexibility, as previously reported [27]. The difference was that the internalized LYC significantly interfered the oxidation nucleation of iron into rHuHF cavity. Thus, more black uranium acetate was entered into the cavity of rHuHF-LYC when the protein spheres were negatively stained for TEM imaging (Figure 1E). This demonstrated that LYC molecules were successfully inserted into rHuHF cavity, accompanied by the greatly change of the solubility of LYC. And the encapsulation benefited the stability of LYC molecule against the affecting factors in external systems, since the secondary structure and particle size of rigid rHuHF nanocages with nearly the same size remained unchanged after embedding (Figures 1F and G), which might provide the physical barrier and chemical stabilization effect for the loaded LYC molecules.

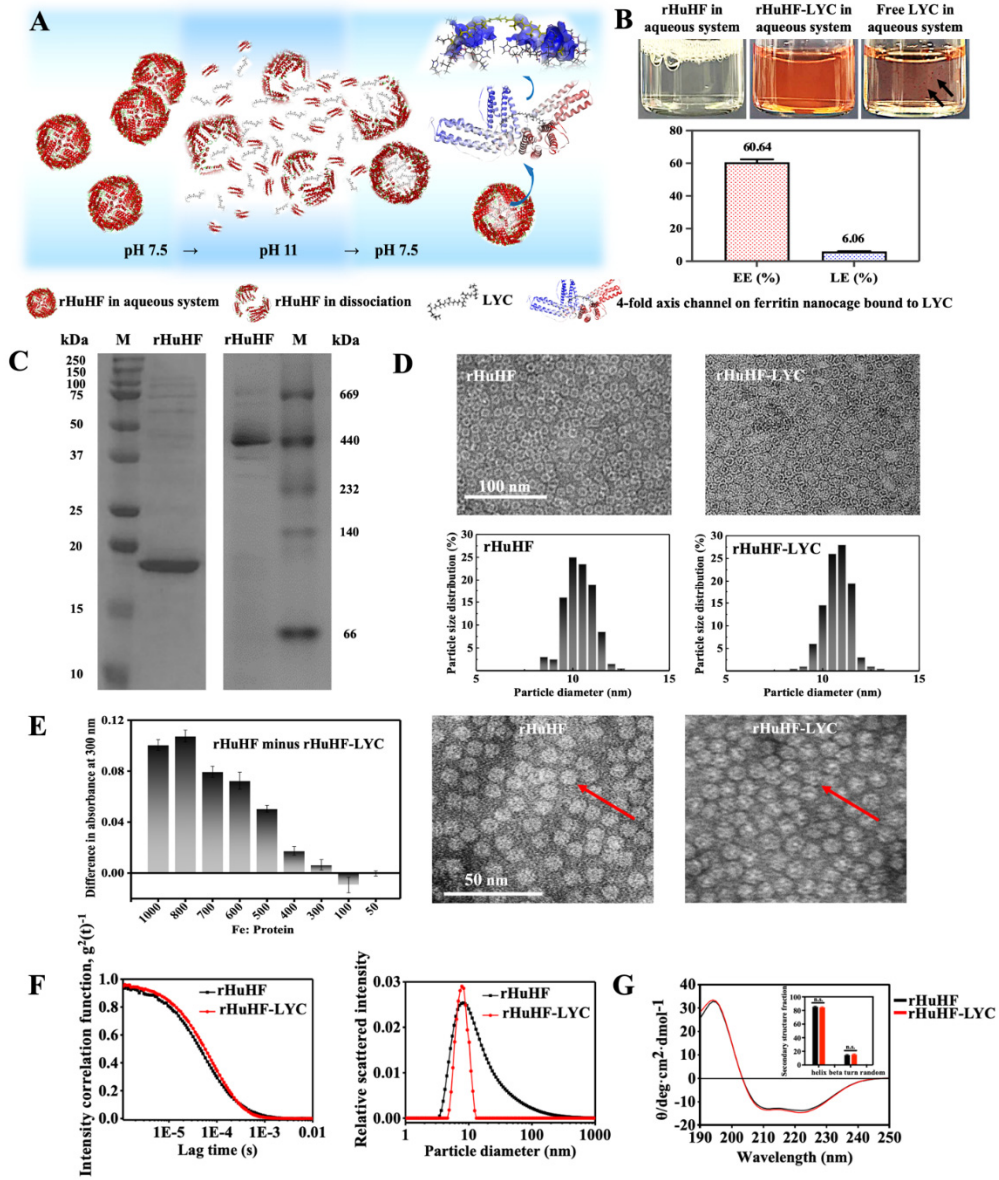

Figure 1. Construction and characterization of rHuHF-LYC nanoparticles. A) Morphological change during the encapsulation of LYC molecules based on the rHuHF nanocarrier in aqueous systems and 3D simulation of the binding sites at the fourfold axis of the cavity. B) The loading amount of LYC and solution state of rHuHF-LYC. C) SDS-PAGE (left) and Native-PAGE (right) of rHuHF. M: protein markers. D) Morphology and diameter statistics of rHuHF and rHuHF-LYC using TEM imaging. E) Negative stain imaging of nanoparticles after iron oxidation nucleation in the rHuHF cavity. F) The hydrodynamic diameter distribution and normalized intensity correlation function of nanoparticles. G) Circular dichroism spectrum and secondary structure fraction of rigid rHuHF nanocages and rHuHF-LYC nanoparticles.

3.2. The interaction between LYC and its protein cage to stabilize the LYC molecules

Due to the easy degradability and strong antioxidant capacity of LYC engaging extensive use in healthy function food, its stability does need to be enhanced against the loss of its biological properties. The rigid rHuHF nanocages stabilized LYC molecules as the protective barriers keeping away the affecting factors in external systems, accompanied by a great melioration in the thermal stability and antioxidant capacity of rHuHF-LYC compared with free LYC (Figures 2A and 2B). The regression coefficients (R^2) of the thermal degradation kinetics were 0.9558 (control) and 0.9945 (rHuHF-LYC), respectively, declaring nice correlation between the degradation residue of LYC and reaction time. LYC level in rHuHF-LYC nanoparticle remained stable at around 85% of the initial level when the degradation slowed down while that in free LYC group was only 78% at 7 h, indicating that the LYC encapsulation of rHuHF works on the protection of LYC from heat. Furthermore, the DPPH inhibition of rHuHF-LYC group significantly increased when the reaction time exceeds 60 min, far outstripping the control group of free LYC. The results fully demonstrated that the antioxidant capacity of LYC encapsulated in rHuHF nanocages was well maintained over time because of the protection of shell-like ferritin nanocages. These also suggested the possible interaction between the LYC molecule and its protein cage that contributes to the stability of LYC molecule.

The interactions between LYC molecules and their rHuHF nanocages were first simulated and calculated by molecular docking. The results with high CDOCKER energy (−ECD) showed that the binding sites of LYC located in the lumen of rHuHF-LYC nanocages near the fourfold axis channels and consisted of ALA47, LYS49, and LYS172 to form hydrophobic bonds (Figure 2C and Table S1). The binding force might promote the successful encapsulation of LYC molecules into ferritin nanocages, causing the stability and solubility of LYC induced by their interaction. Moreover, the equilibrium thermal change and its parameters of rHuHF and LYC were measured via ITC. The fitted curve from the raw revealed the binding of rHuHF and LYC (Figure 2D). The ΔH (enthalpy), ΔS (entropy), ΔG (not shown), Kd (binding constant), and n (the apparent binding stoichiometry) values for the reaction were −1826 $kJ \cdot mol^{-1}$, −6002 $J \cdot mol^{-1} \cdot K^{-1}$, −37.4 $kJ \cdot mol^{-1}$, 4.572×10^{-7} M, and 1.193, respectively. ΔH and ΔS were negative, indicating favorable noncovalent interactions between rHuHF and LYC. Accordingly, the binding reaction could be non-specific, exothermic ($\Delta H < 0$), and spontaneous ($\Delta G < 0$) binding reaction. These results illustrated the LYC encapsulation into rHuHF nanocages resulted in the stability and solubility of LYC induced by their interactions.

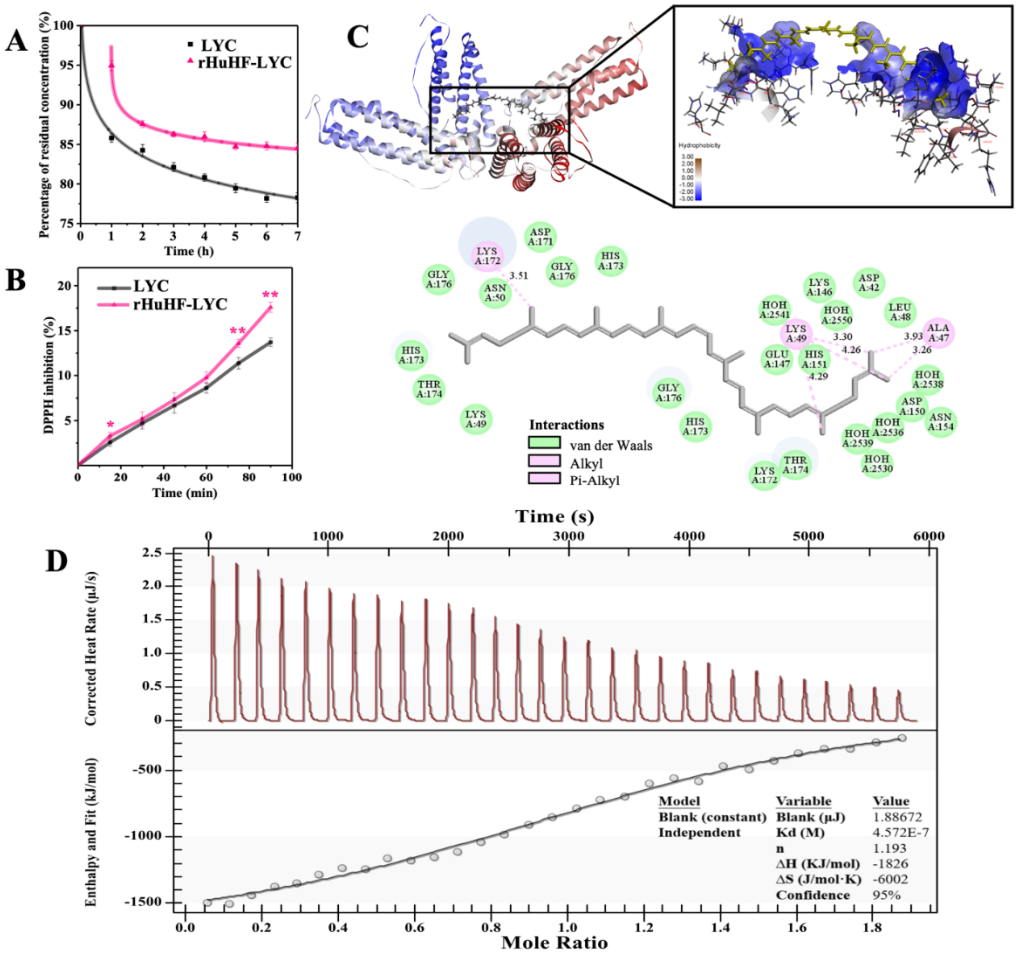

Figure 2. A) The thermal stability of LYC alone and LYC in rHuHF showed by decay kinetic curves under 37 °C. B) DPPH inhibition of LYC alone and LYC encapsulated within rHuHF as a function of time with the detection wavelength at 520 nm. Values are means ± SD (n = 3), student's t-test, ** $P < 0.01$. C) The 3D structure and 2D diagram of the docking position of LYC and rHuHF. D) ITC validation for the interaction of LYC with rHuHF.

3.3. Transcytosis across the BBB and evaluation of the neuron-targeting ability

The rHuHF acts as the optimal nanocarrier across BBB through endogenous receptor-mediated transport (RMT) [15] in virtue of transferrin receptor 1 (TfR1), which is abundant on BBB endothelial cells (ECs). It permits rHuHF to transfer cross BBB via the endosomal compartment. To verify the BBB penetration of the rHuHF-LYC nanocomplex, we performed a BBB transcytosis test. FITC-rHuHF-LYC was added to the upper chamber of human or mouse BBB ECs based on confirming that it does not affect the survival of cells (Figures 3A and 3B). FITC-rHuHF-LYC, but not FITC-LFn (control human L-ferritin), significantly traversed human or mouse BBB ECs, and the transcytosis efficiency of FITC-rHuHF-LYC in bEnd.3 and hCMEC/D3 cells was almost five times higher than FITC-LFn over 1 h (Figures 3C and 3D). The absorption of FITC-rHuHF-LYC in the lower PC12 cells was significantly increased after 2 h (Figures 3E and 3F). Moreover, the fluorescence co-imaging of FITC-rHuHF-LYC and lysosomes showed their non-colocalization with Pearson correlation coefficients of -0.11 and 0.16, respectively, indicating that FITC-rHuHF-LYC was not absorbed but transported in BBB ECs (Figure 3G). These results demonstrated the ability of rHuHF-LYC to traverse the BBB *in vitro*. Moreover, FITC-rHuHF-LYC was significantly absorbed by PC12 cells and colocalized with lysosomes (Figures 3H and 3J), with a Pearson correlation coefficient of 0.73 (Figure 3I), indicating that FITC-rHuHF-LYC could enter nerve cells. It was consistent

with the transcytosis results of BBB ECs transwells, which jointly proved that FITC-rHuHF-LYC could be absorbed by nerve cells.

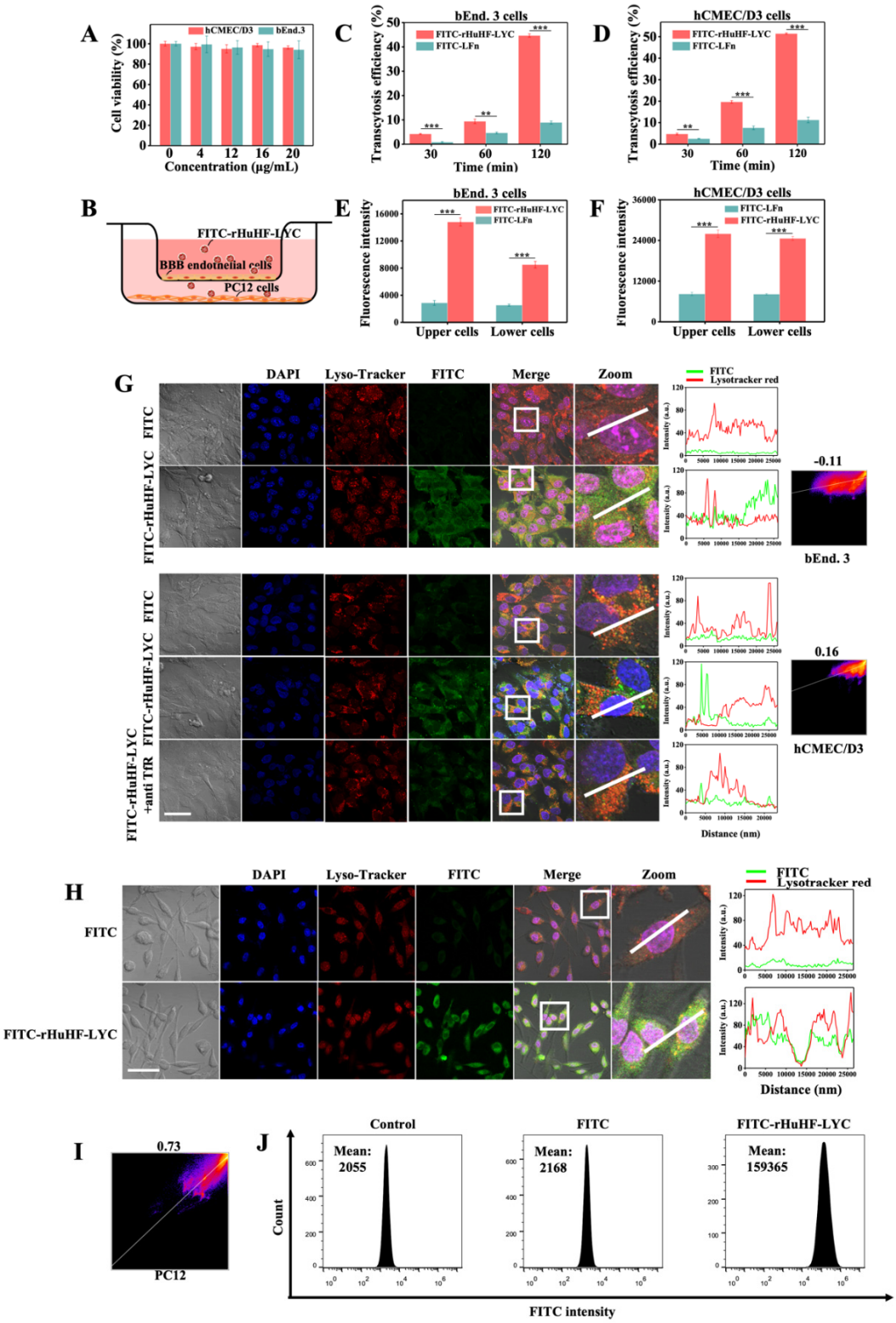

Figure 3. Transcytosis capacity of rHuHF-LYC across the BBB. A) Cell viabilities of bEnd.3 and hCMEC/D3 cells incubating with FITC-rHuHF-LYC. Means ± the standard deviations, n = 6. B) Illustration of the transwell chamber as BBB model *in vitro*. C, D) Transcytosis of FITC-rHuHF-LYC/FITC-LFn in the BBB ECs. E, F) Absorption of FITC-rHuHF-LYC in upper (BBB endothelium) and lower (PC12) cells after 2 h. Means ± the standard deviations, n = 3, student's t-test, $^{**}P < 0.01$, $^{***}P < 0.001$. G) The fluorescence co-imaging of FITC-rHuHF-LYC (green) and lysosome (red) in BBB ECs. Scale bar: 50 μm. H) The fluorescence co-imaging of FITC-rHuHF-LYC (green) and lysosome (red) in PC12 cells. Scale bar: 50 μm. I) The Pearson correlation coefficient of colocalization between FITC-rHuHF-LYC and lysosome in PC12 cells. J) The uptaking quantification of FITC-rHuHF-LYC in PC12 cells for 2 h using flow cytometry (n = 3 per group).

3.4. rHuHF-LYC nanoparticle as intracellular ROS scavenger in neurons

In the neuronal microenvironment, oxidative damage antecedes the occurrence of neuropathology, causing further damage in mitochondria and even cognitive decline. Several studies have highlighted the D-gal-based model for inducing brain aging and neuronal apoptosis [1, 28]. Herein, BV2 and PC12 cells were cultured to investigate the peroxidation alleviation via rHuHF-LYC on D-gal-induced damage. Moreover, 500 mmol/L D-gal resulted in BV2 and PC12 cells reaching approximately IC50. Expectedly, the addition of rHuHF-LYC significantly reduced ROS levels in a dose-dependent manner in PC12 cells ($P < 0.05$), which is superior to rHuHF alone (Figure 4A). Also, the modulation of intracellular SOD activity by rHuHF-LYC was verified in PC12 cells (Figure 4B), and rHuHF-LYC at 20 μg/mL and above significantly attenuated the D-gal-induced decrease in SOD activity ($P < 0.05$). Similarly, the strong ROS signals of PC12 and BV2 cells induced by D-gal were weakened and gradually approached the fluorescence intensity of the control group due to rHuHF-LYC treatment (Figures 4C, E, F and S1), which also alleviated the morphological shrinkage and tendency to apoptosis of BV2 and PC12 cells (Figure 4D). These results indicated that rHuHF-LYC nanoparticles attenuated D-gal-induced cellular peroxidation.

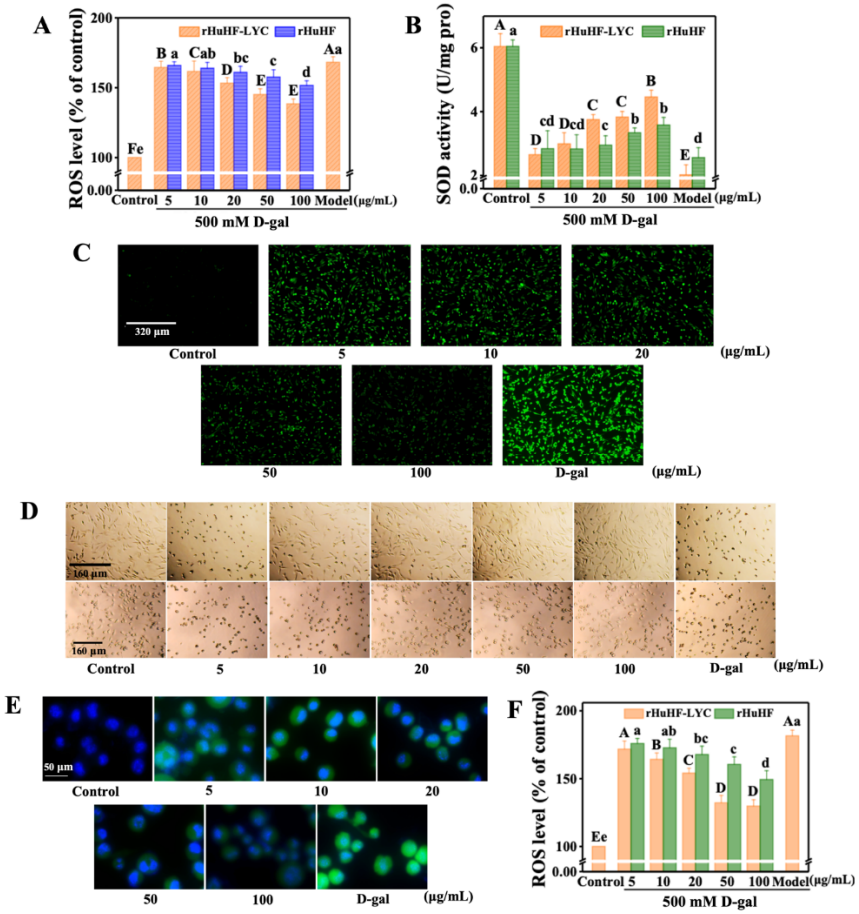

Figure 4. Protection of rHuHF-LYC against D-gal-induced cell injury on BV2 and PC12 cells. A) Statistics of ROS intensity in PC12 cells treated with rHuHF/rHuHF-LYC. B) SOD activities of cells treated with rHuHF/rHuHF-LYC. C) Fluorescence imaging of ROS intensity. D) Morphological restoration of PC12 and BV2 cells treated with rHuHF-LYC. E) Fluorescence imaging of ROS levels in BV2 cells treated with rHuHF-LYC. F) Quantitative statistics of fluorescence generated by BV2 cells treated with rHuHF/rHuHF-LYC. Means ± SD with one-way ANOVA analysis, the difference among groups was statistically significant: different uppercase/lowercase represented $P < 0.05$; the same uppercase/lowercase represented $P < 0.05$.

Moreover, rHuHF-LYC significantly alleviated the apoptosis of BV2 and PC12 cells, characterized by changes in the mitochondrial membrane potential and phosphatidylserine evagination (Figures 5A). As shown by fluorescence imaging and quantitative analysis, the addition of rHuHF-LYC was beneficial for maintaining full cell morphology (pink and blue), reducing fragmentation or apoptosis (green), and maintaining cell adhesion. And the number of apoptotic PC12 cells was significantly suppressed by rHuHF-LYC in a dose-dependent manner ($P < 0.05$) (Figures 5B). Therefore, the nutritional and protective effects of BV2 cells on neurons were weakened under D-gal interference, while rHuHF-LYC plays a direct role in protecting neurons while repairing these undesirable changes. Furthermore, AChE and ACh are both key substances in the cholinergic system and play important roles in evaluating the condition of nerve cells. rHuHF-LYC significantly inhibited the increase in AChE activity and decrease in ACh activity after D-gal injury in BV2 and PC12 cells ($P < 0.05$), which alleviated the reduction or termination of excitation in nerve cells induced by D-gal (Figures 5C and 5D). These results demonstrated that the nanoparticles played a crucial role in protecting BV2 and PC12 cells via upholding the antioxidant defenses and mitochondrial function.

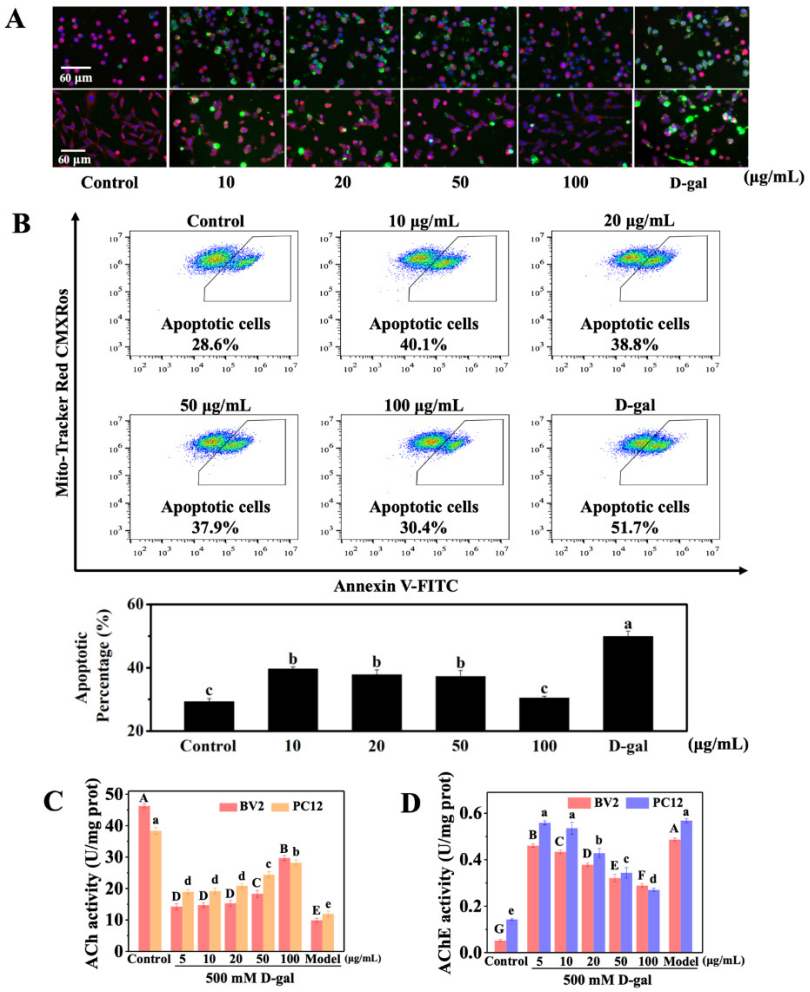

Figure 5. Alleviation of the loss of mitochondrial membrane potential and neuronal apoptosis via rHuHF-LYC treatment. A) Mitochondrial membrane potential imaging of PC12 and BV2 cells treated with rHuHF-LYC. B) Apoptosis results of PC12 cells treated with rHuHF-LYC was measured using flow cytometry; cells were stained with Mito-Tracker Red CMXRos/Annexin-FTIC (n = 3). C-D) The ACh content and AChE activity in BV2 and PC12 cells treated with rHuHF-LYC (n = 6). Means ± SD with one-way ANOVA analysis, the difference among groups was statistically significant: different uppercase/lowercase represented $P < 0.05$; the same uppercase/lowercase represented $P < 0.05$.

3.5. Regulating the expression of apoptosis-related proteins in PC12 cells via rHuHF-LYC treatment

Intracellular excessive oxidation is an early trigger of neuronal apoptosis, because the signal transmission of the nervous system requires a large amount of energy support, and excessive ROS is accompanied by the sharp decline in intracellular energy support and subsequent initiation of apoptosis [29]. It has been confirmed that D-gal damages the antioxidant capacity of nerve cells and increases the apoptosis rate of neurons, thus inducing a marked increase in the expression levels of Bax, caspase-3, caspase-9 and other pro-apoptosis factors and a decrease in the expression level of Bcl-2 [30, 31]. Therefore, it is essential to investigate the cascade mechanism of apoptosis-related signalling proteins to assess the occurrence of neuronal apoptosis. The signature pro-/anti-apoptotic and senescence-associated proteins were detected by western blotting (Figure 6) and the regulatory mechanisms of rHuHF-LYC in the neural microenvironment were shown in Figure 7.

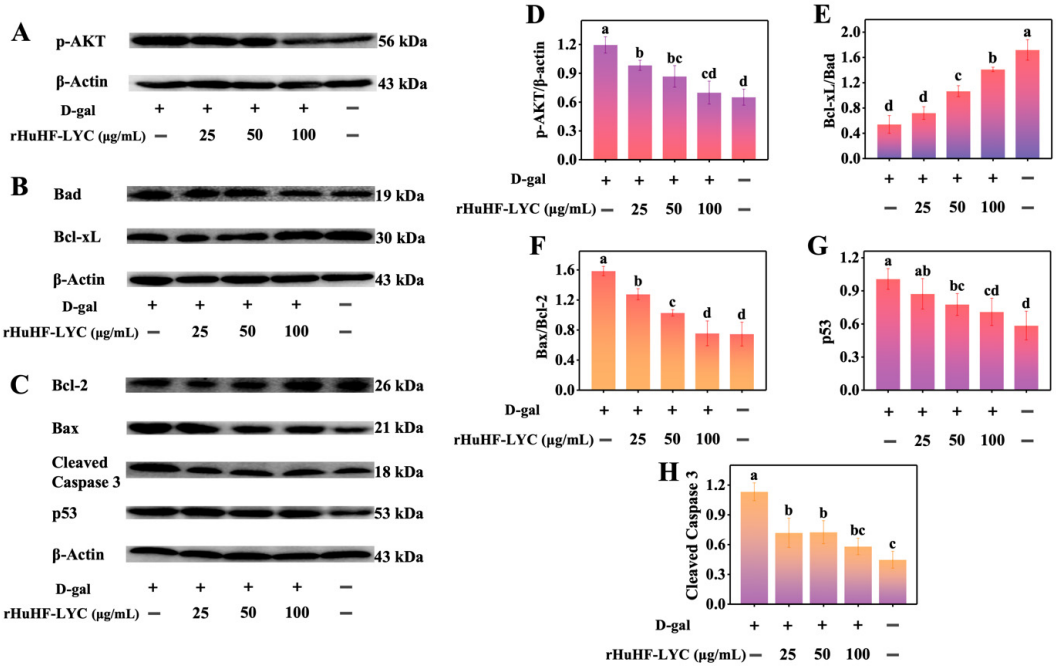

Figure 6. Effects of rHuHF-LYC on the expression level of proteins related to neuron apoptosis in PC12 cells by western blot analysis. A-C) Immunoblotting bands of neuron apoptosis related proteins. D-H) Relative quantification of neuron apoptosis related proteins (n = 3). Means ± SD, the difference among groups was statistically significant: different uppercase/lowercase represented $P < 0.05$; the same uppercase/lowercase represented $P < 0.05$.

The immunoblotting bands and their relative quantification demonstrated that rHuHF-LYC nanoparticles significantly up-regulated intracellular levels of Bcl-xL and Bcl-2 compared to the model group ($P < 0.05$), as well as significantly down-regulated the expressions of p-AKT, Bad, Bax, Cleaved Caspase-3 and p53. In response to rHuHF-LYC treatment, the down-regulated p-AKT levels in PC12 cells caused the mitochondria-mediated increase of Bcl-xL/Bad value and reduction of Bax/Bcl-2. Finally, these modifications elicited the significant downregulation of Cleaved Caspase-3 and p53 ($P < 0.05$), revealing the inhibitory regulation of neuronal apoptosis via rHuHF-LYC treatment. In a word, rHuHF-LYC slowed down neuronal apoptosis of PC12 cells through regulating the expression levels of intracellular apoptosis-related proteins.

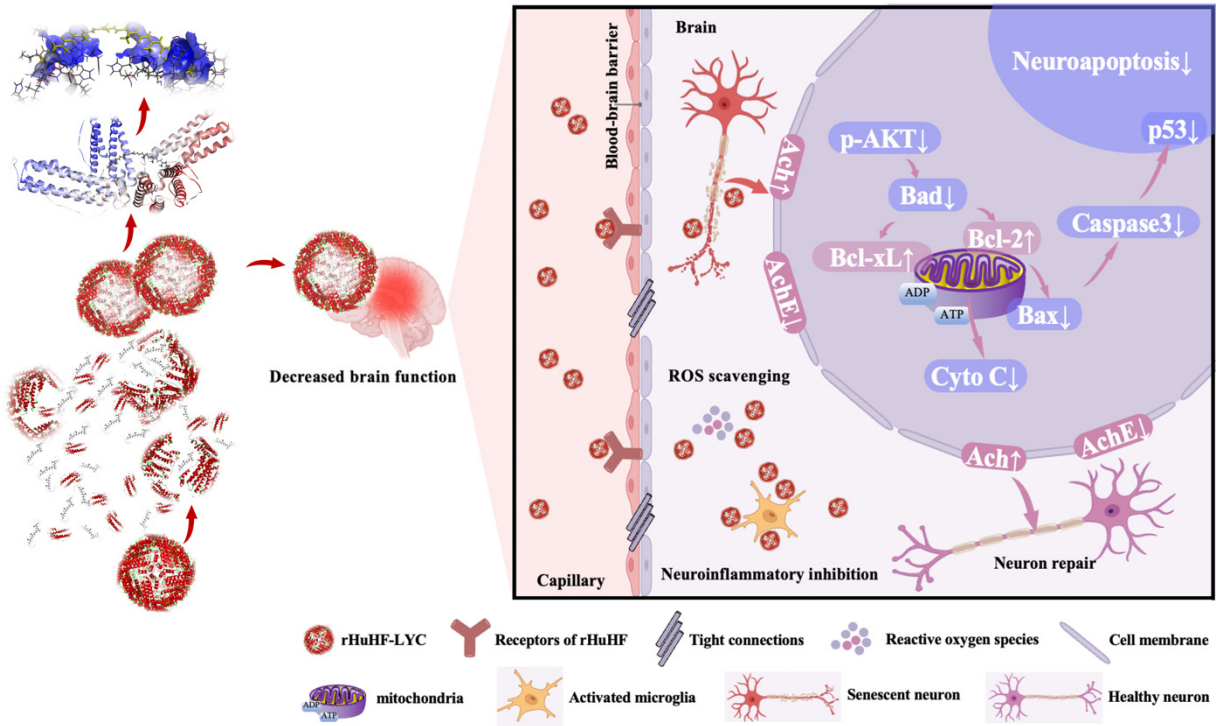

Figure 7. Schematic diagram showing the regulating mechanism of nanoparticles in neural microenvironment: 1) BBB transcytosis and nerve cell uptaking via RMT process; 2) alleviation the intracellular oxidation levels and the decreased mitochondrial membrane potential; 3) neuroprotection achieved via attenuating apoptosis and improving cholinergic levels of nerve cells.

4. Conclusions

In summary, the rHuHF-LYC nanoparticles constructed with the ability to scavenge neural ROS exhibited excellent performance through protecting neurons and improving the neural microenvironment. rHuHF-LYC crossed the BBB via the RMT process and were internalized into neurons. Subsequently, the excessive oxidation and mitochondrial homeostasis imbalance in PC12 and BV2 cells were alleviated. Moreover, rHuHF-LYC slowed down neuronal apoptosis of PC12 cells through regulating the expression levels of intracellular apoptosis-related proteins. Therefore, rHuHF-LYC nanoparticle inhibits the development of an undesirable neuronal microenvironment and provides a promising treatment option to combat brain aging.

Declaration of competing interest

The authors declare no competing financial interest.

Acknowledgment

This study was financially supported by the National Natural Science Foundation of China (31730069) and Graduate Innovation Fund of Dalian Polytechnic University. We would like to thank Editage (www.editage.cn) for English language editing.

References

[1] S. Lu, J. Zhou, C. Yang, X. Zhang, Y. Shi, J. Liu, X. Yan, J. Liang, X. Liu, L. Luo, D. Zhou, Z. Yin, gamma-Glutamylcysteine ameliorates D-gal-induced senescence in PC12 cells and mice via activating AMPK and SIRT1, Food Funct 13(14) (2022) 7560-7571.

[2] Y. Zhang, A. Khalique, X. Du, Z. Gao, J. Wu, X. Zhang, R. Zhang, Z. Sun, Q. Liu, Z. Xu, A.C. Midgley, L. Wang, X. Yan, J. Zhuang, D. Kong, X. Huang, Biomimetic Design of Mitochondria-Targeted Hybrid Nanozymes as Superoxide Scavengers, Adv Mater 33(9) (2021) e2006570.

[3] P. Liu, T. Zhang, Q. Chen, C. Li, Y. Chu, Q. Guo, Y. Zhang, W. Zhou, H. Chen, Z. Zhou, Y. Wang, Z. Zhao, Y. Luo, X. Li, H. Song, B. Su, C. Li, T. Sun, C. Jiang, Biomimetic Dendrimer-Peptide Conjugates for Early Multi-Target Therapy of Alzheimer's Disease by Inflammatory Microenvironment Modulation, Adv Mater 33(26) (2021) e2100746.

[4] F. Zeng, Y. Wu, X. Li, X. Ge, Q. Guo, X. Lou, Z. Cao, B. Hu, N.J. Long, Y. Mao, C. Li, Custom-Made Ceria Nanoparticles Show a Neuroprotective Effect by Modulating Phenotypic Polarization of the Microglia, Angew Chem Int Ed Engl 57(20) (2018) 5808-5812.

[5] X. Bai, S. Wang, X. Yan, H. Zhou, J. Zhan, S. Liu, V.K. Sharma, G. Jiang, H. Zhu, B. Yan, Regulation of Cell Uptake and Cytotoxicity by Nanoparticle Core under the Controlled Shape, Size, and Surface Chemistries, ACS Nano 14(1) (2020) 289-302.

[6] T. Liu, B. Xiao, F. Xiang, J. Tan, Z. Chen, X. Zhang, C. Wu, Z. Mao, G. Luo, X. Chen, J. Deng, Ultrasmall copper-based nanoparticles for reactive oxygen species scavenging and alleviation of inflammation related diseases, Nat Commun 11(1) (2020) 2788.

[7] L. Zhang, C. Chen, M.S. Mak, J. Lu, Z. Wu, Q. Chen, Y. Han, Y. Li, R. Pi, Advance of sporadic Alzheimer's disease animal models, Med Res Rev 40(1) (2020) 431-458.

[8] Y. Sang, F. Zhang, H. Wang, J. Yao, R. Chen, Z. Zhou, K. Yang, Y. Xie, T. Wan, H. Ding, Apigenin exhibits protective effects in a mouse model of d-galactose-induced aging via activating the Nrf2 pathway, Food Funct 8(6) (2017) 2331-2340.

[9] M. Qu, Z. Zhou, C. Chen, M. Li, L. Pei, F. Chu, J. Yang, Y. Wang, L. Li, C. Liu, L. Zhang, G. Zhang, Z. Yu, D. Wang, Lycopene protects against trimethyltin-induced neurotoxicity in primary cultured rat hippocampal neurons by inhibiting the mitochondrial apoptotic pathway, Neurochem Int 59(8) (2011) 1095-103.

[10] M. Qu, X. Nan, Z. Gao, B. Guo, B. Liu, Z. Chen, Protective effects of lycopene against methylmercury-induced neurotoxicity in cultured rat cerebellar granule neurons, Brain Res 1540 (2013) 92-102.

[11] D. Chen, C. Huang, Z. Chen, A review for the pharmacological effect of lycopene in central nervous system disorders, Biomed Pharmacother 111 (2019) 791-801.

[12] M.T. Lee, B.H. Chen, Stability of lycopene during heating and illumination in a model system, Food Chemistry 78(4) (2002) 425-432.

[13] M. Caseiro, A. Ascenso, A. Costa, J. Creagh-Flynn, M. Johnson, S. Simões, Lycopene in human health, Lwt 127 (2020).

[14] L. Cai, C. Yang, W. Jia, Y. Liu, R. Xie, T. Lei, Z. Yang, X. He, R. Tong, H. Gao, Endo/Lysosome-Escapable Delivery Depot for Improving BBB Transcytosis and Neuron Targeted Therapy of Alzheimer's Disease, Advanced Functional Materials 30(27) (2020).

[15] K. Fan, X. Jia, M. Zhou, K. Wang, J. Conde, J. He, J. Tian, X. Yan, Ferritin Nanocarrier Traverses the Blood Brain Barrier and Kills Glioma, ACS Nano 12(5) (2018) 4105-4115.

[16] M. Liang, K. Fan, M. Zhou, D. Duan, J. Zheng, D. Yang, J. Feng, X. Yan, H-ferritin-nanocaged doxorubicin nanoparticles specifically target and kill tumors with a single-dose injection, Proc Natl Acad Sci U S A 111(41) (2014) 14900-5.

[17] Y. Li, L. Dong, Z. Mu, L. Liu, J. Yang, Z. Wu, D. Pan, L. Liu, Research Advances of Lactoferrin in Electrostatic Spinning, Nano Self-Assembly, and Immune and Gut Microbiota Regulation, J Agric Food Chem 70(33) (2022) 10075-10089.

[18] K. Fan, M. Zhou, X. Yan, Questions about horse spleen ferritin crossing the blood brain barrier via mouse transferrin receptor 1, Protein Cell 8(11) (2017) 788-790.

[19] S. Zhao, H. Duan, Y. Yang, X. Yan, K. Fan, Fenozyme Protects the Integrity of the Blood-Brain Barrier against Experimental Cerebral Malaria, Nano Lett 19(12) (2019) 8887-8895.

[20] L. Chen, G. Bai, R. Yang, J. Zang, T. Zhou, G. Zhao, Encapsulation of beta-carotene within ferritin nanocages greatly increases its water-solubility and thermal stability, Food Chem 149 (2014) 307-12.

[21] X. Xia, X. Tan, C. Wu, Y. Li, G. Zhao, M. Du, PM1-loaded recombinant human H-ferritin nanocages: A novel pH-responsive sensing platform for the identification of cancer cells, Int J Biol Macromol 199 (2022) 223-233.

[22] L. Chen, G. Bai, S. Yang, R. Yang, G. Zhao, C. Xu, W. Leung, Encapsulation of curcumin in recombinant human H-chain ferritin increases its water-solubility and stability, Food Research International 62 (2014) 1147-1153.

[23] H. Sun, Y. Zhong, X. Zhu, H. Liao, J. Lee, Y. Chen, L. Ma, J. Ren, M. Zhao, M. Tu, F. Li, H. Zhang, M. Tian, D. Ling, A Tauopathy-Homing and Autophagy-Activating Nanoassembly for Specific Clearance of Pathogenic Tau in Alzheimer's Disease, ACS Nano 15(3) (2021) 5263-5275.

[24] J. Zang, H. Chen, G. Zhao, F. Wang, F. Ren, Ferritin cage for encapsulation and delivery of bioactive nutrients: From structure, property to applications, Crit Rev Food Sci Nutr 57(17) (2017) 3673-3683.

[25] C. Gu, T. Zhang, C. Lv, Y. Liu, Y. Wang, G. Zhao, His-Mediated Reversible Self-Assembly of Ferritin Nanocages through Two Different Switches for Encapsulation of Cargo Molecules, ACS Nano 14(12) (2020) 17080-17090.

[26] R. Yang, Z. Zhou, G. Sun, Y. Gao, J. Xu, P. Strappe, C. Blanchard, Y. Cheng, X. Ding, Synthesis of homogeneous protein-stabilized rutin nanodispersions by reversible assembly of soybean (Glycine max) seed ferritin, RSC Advances 5(40) (2015) 31533-31540.

[27] S. Zhang, J. Zang, H. Chen, M. Li, C. Xu, G. Zhao, The Size Flexibility of Ferritin Nanocage Opens a New Way to Prepare Nanomaterials, Small 13(37) (2017).

[28] Y. Liu, Y. Liu, Y. Guo, L. Xu, H. Wang, Phlorizin exerts potent effects against aging induced by D-galactose in mice and PC12 cells, Food Funct 12(5) (2021) 2148-2160.

[29] J. Dohla, E. Kuuluvainen, N. Gebert, A. Amaral, J.I. Englund, S. Gopalakrishnan, S. Konovalova, A.I. Nieminen, E.S. Salminen, R. Torregrosa Munumer, K. Ahlqvist, Y. Yang, H. Bui, T. Otonkoski, R. Kakela, V. Hietakangas, H. Tyynismaa, A. Ori, P. Katajisto, Metabolic determination of cell fate through selective inheritance of mitochondria, Nat Cell Biol 24(2) (2022) 148-154.

[30] Y. Zhang, H. Li, X. Yang, G. Jin, Y. Zhang, Cognitive-enhancing effect of polysaccharides from Flammulina velutipes on Alzheimer's disease by compatibilizing with ginsenosides, Int J Biol Macromol 112 (2018) 788-795.

[31] C.M. Lin, Y.T. Lin, T.L. Lee, Z. Imtiyaz, W.C. Hou, M.H. Lee, In vitro and in vivo evaluation of the neuroprotective activity of Uncaria hirsuta Haviland, J Food Drug Anal 28(1) (2020) 147-158.